Macromolecules
ARTICLE

Macromolecules **2009**, *42*, 4795–4800 **4795**
DOI: 10.1021/ma900503h

In Situ Observation of Tensile Deformation Processes of Soft Colloidal Crystalline Latex Fibers

Jianqi Zhang,[†] Shanshan Hu,[†] Jens Rieger,[‡] Stephan V. Roth,[§] Rainer Gehrke,[§] and Yongfeng Men*,[†]

[†]*State Key Laboratory of Polymer Physics and Chemistry, Changchun Institute of Applied Chemistry, Chinese Academy of Sciences, Graduate University of Chinese Academy of Sciences, Renmin Street 5625, 130022 Changchun, P.R. China,* [‡]*BASF SE, Polymer Physics, 67056 Ludwigshafen, Germany, and* [§]*HASYLAB am DESY, Notkestrasse 85, 22607 Hamburg, Germany*

Received March 9, 2009; Revised Manuscript Received April 11, 2009

ABSTRACT: The deformation mechanism of styrene/*n*-butyl acrylate copolymer latex films with fiber symmetric crystalline structure subjected to uniaxial stretching was studied using synchrotron small-angle X-ray scattering technique. The fibers were drawn at angles of 0, 35, and 55° with respect to the fiber axis. In all cases, the microscopic deformation within the crystallites was found to deviate from affine deformation behavior with respect to the macroscopic deformation ratio. Moreover, the extent of this deviation is different in the three cases. This peculiar behavior can be attributed to the relative orientation of the (111) plane of the crystals, the plane of densest packing, with respect to the stretching direction in each case. When the stretching direction coincides with the crystallographic (111) plane, which is the case for stretching directions of 0 and 55° with respect to the fiber axis, the microscopic deformation deviates less from affine behavior than when the stretching direction is arbitrarily oriented with respect to the crystallographic (111) plan. The dependence of tilting angle and *d*-spacing of selected (111) or (220) planes from the microscopic crystalline draw ratio are fully in accordance with theoretical considerations.

Introduction

Polymeric latex dispersions typically consist of polymeric particles with a diameter of about 100 nm that are dispersed in water. These dispersions are widely used in many applications, such as paints, paper coatings, adhesives, etc.[1] When an aqueous dispersion of soft polymeric particles dries under suitable conditions a transparent void-free film with colloidal crystalline structure is formed. Although the microscopic details of film formation are still a topic of considerable debate, the film formation process is usually considered in terms of three sequential steps: increasing particle concentration and crystalline ordering of the polymeric particles, particle deformation and polymer chain diffusion across particle boundaries.[2,3] Latex particles usually pack in a face-centered cubic (fcc) structure and assume a dodecahedral shape in the deformed state.[4−8]

The film formation processes of hard or soft colloidal particles have been widely studied using microscopic and spectroscopic techniques.[9−15] However, relatively few studies dealt with the deformation mechanisms of polymer latex films with respect to its microstructure evolution under macroscopic stress. The deformation of hybrid films filled with inorganic nanoparticles has been studied.[16−21] A theoretical model was presented based on experiments using small-angle neutron scattering (SANS).[16,22] The deformation mechanism of these composite films, containing silica nanoparticles, was dependent on the pH value of the latex dispersions, the silica volume fraction and the size of silica particles.[17] Lepizzera et al. presented evidence for two modes of deformation based on atomic force microscopy studies on deformed core/shell latex films: matrix deformation and geometric rearrangement.[18,19] Different deformation modes were discussed for the polymer composite films with random and periodic structures.[20] The deformation of the films made from the polymeric particles was affine when the films were stretched in the dry state, while the deformation was nonaffine when the films were stretched in the wet state. In the latter case the macroscopic stress induced microscopic shear deformation, i.e., the particles slipped past each other.[21] In our previous work,[23,24] synchrotron small-angle X-ray scattering (SAXS) was used to study the deformation mechanism of soft latex films. The latex films used in our studies contain nonpolymeric material such as salt and surfactants that is located in the interstices between the closely packed particles thus providing the electron density difference necessary. It was found that the crystalline lattice constants changed considerably during macroscopic deformation, resulting not only in the deformation of the crystallographic structure but also in considerable nonaffine deformation at high draw ratios. The deformation behavior of the latex films changed from nonaffine to affine deformation with increasing annealing temperature. However, up to now, only isotropic polycrystalline structures were considered experimentally. A detailed interpretation of the deformation mechanisms based on such isotropic samples is difficult because the existence of crystallites with all orientations make it impossible to separate scattering signals from individual crystallites with specific orientations. Recently, we succeeded in preparing bulk soft colloidal crystals with fiber symmetry.[26] Such samples allow to study the deformation mechanisms in more detail since the crystals have a preferential orientation.

In the present work, the deformation mechanism of a soft colloidal crystalline styrene/*n*-butyl acrylate copolymer latex film with a fiber symmetry subjected to stretching was investigated by in situ synchrotron SAXS. In order to clarify the detailed deformation mechanism of the oriented latex colloidal crystalline film, the samples were stretched along different directions with

*Corresponding author. E-mail: men@ciac.jl.cn.

Published on Web 04/29/2009

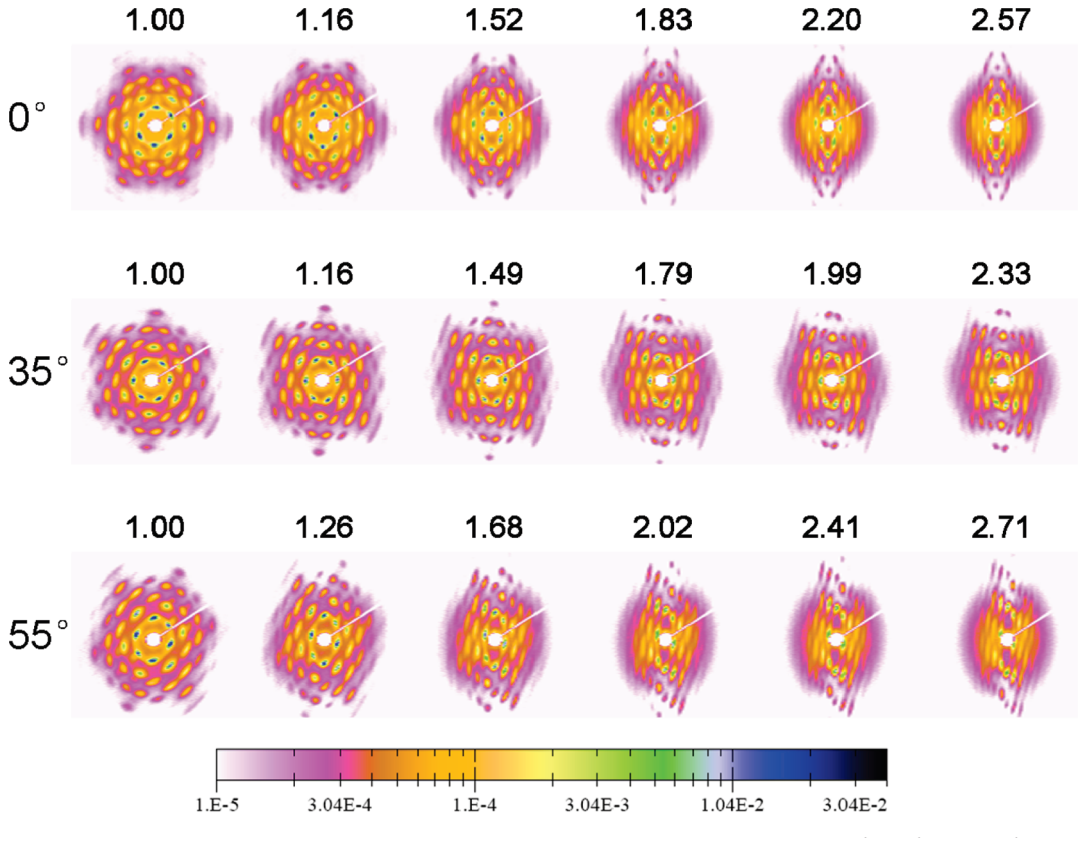

Figure 1. Selected SAXS patterns of latex films being uniaxially drawn at 0, 35, and 55° with respect to the fiber axis. The macroscopic draw ratio is indicated at each pattern. The tensile stretching direction is horizontal.

respect to the fiber axis. It was found that the extent of the nonaffine deformation of the crystallites with respect to the macroscopic deformation depended on the stretching directions. The deformation of the colloidal crystalline structure can be interpreted by simple geometrical considerations.

Experimental Section

A styrene/*n*-butyl acrylate copolymer (PS-*co*-BA) latex dispersion with a solid content of ca. 25 wt % was used in the present work. A detailed description of the latex dispersion can be found elswhere.[24,26,27] The glass-transition temperature of this PS-*co*-BA is about 20 °C. The particle size of the latex dispersion was 118 nm as determined by SAXS. The 25 wt % dispersion was dried in a rectangular Kapton tube with a length, width and height of 25, 6, and 1 mm, respectively, at room temperature (25 °C) with a humidity of 30%. The tube was placed horizontally during sample preparation. Such a process always results in an asymmetric behavior where the system starts to solidify at one side of the tube and the dispersion on the other side remains liquid and moves inside. It has been confirmed that due to the convective flow of the water during evaporation, the latex particles in the liquid phase were driven to pack onto the existing solid phase.[26] A transparent, mechanically stable solid sample with a size of about 1 mm in thickness and 5 mm in length was obtained after complete evaporation of the water after a week.

Synchrotron SAXS measurements were performed at the beamline BW4 at HASYLAB, DESY, Hamburg, Germany. The energy of the X-ray radiation was 8.979 keV, resulting in a wavelength of 0.13808 nm. The size of the primary X-ray beam at the sample position was 0.4×0.4 mm^2. The sample was mounted onto a tensile tester at the beamline at a sample to detector distance of 5694 mm. At this distance, the effective scattering vector q ($q = (4\pi/\lambda) \sin \theta$, where 2θ is the scattering angle and λ the wavelength) range is $0.03-0.62$ nm^{-1}. The samples were cut into a mini-dog-bone shape before mounting onto the tensile tester and stretched at both ends ensuring that the X-rays were scattered at a fixed position in the middle of the sample. The samples were stretched with a speed of 30 μm/s. The changes in the appearance of the samples during deformation were recorded by a CCD camera as photographs which were used for the calculation of the macroscopic draw ratio. Each SAXS pattern was collected within 60s during a continuous stretching run. The SAXS data were calibrated for background scattering and normalized with respect to the primary beam intensity.

Results and Discussion

Figure 1 shows selected SAXS patterns of uniaxially drawn latex films along different directions with respect to the fiber axis. Three stretching directions were chosen, namely at angles of 0°, 35° and 55° with respect to the fiber axis. The SAXS pattern of the undeformed sample shows a large number of diffraction spots characteristic of an fcc crystalline structure with a fiber symmetry (cf. ref 26). Obviously, the diffraction spots are located on circles with different radii before stretching while they lie on ellipses after drawing. The behavior is very similar the one observed when stretching polycrystalline latex films where the circular intensity distributions (Debye−Scherrer rings) of the undeformed sample change into ellipsoidal intensity distributions of the stretched sample. In the present case the number of diffraction spots remained unchanged upon drawing and the relative scattering intensity of each spot did not changed. When the stretching direction was tilted with respect to the fiber axis, the symmetry of the scattering patterns changed from a fiber symmetry to a centrosymmetry.

Variation of SAXS Patterns. The scattering intensity can be expressed as $I(q) \propto S(q) \times P(q)$, where $S(q)$ is the structure factor due to the crystalline ordering of the latex particles and $P(q)$ is the form factor of the individual particles. Figure 2a presents the SAXS pattern of the fiber symmetric sample (left) and the corresponding theoretical structure

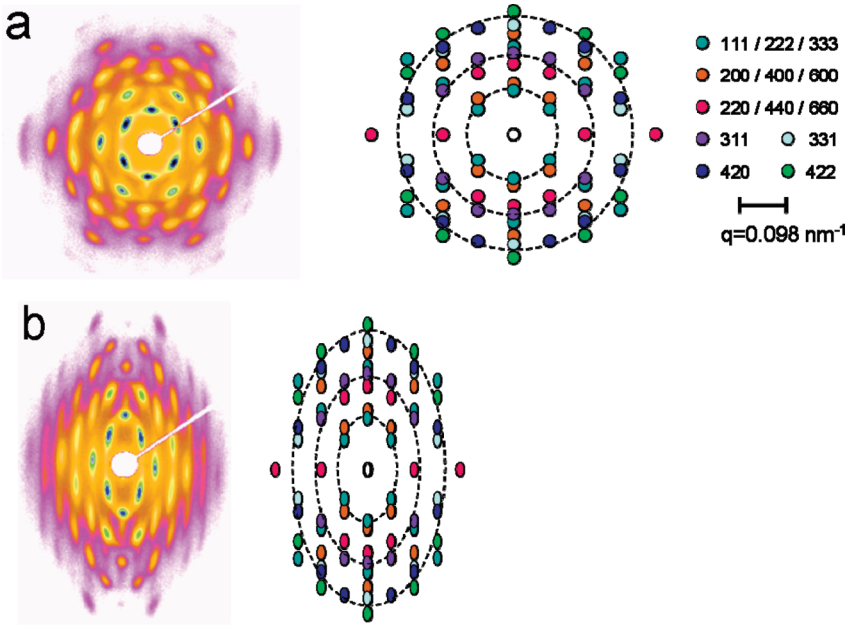

Figure 2. SAXS pattern of the undeformed sample with fiber symmetry (left) and the theoretical structure factor assuming face-centered cubic packing (right) (a); SAXS pattern of the sample that was uniaxially stretched along the fiber axis (left) and the corresponding theoretical structure factor assuming affine deformation (right) (b). Dotted lines denote q values at which the form factor of the latex particle exhibits minima.

factor (right) that is obtained by assuming face-centered cubic (fcc) packing of the spheres. Dashed lines indicate the minimum intensity position of the form factor of the colloidal spheres. The explanation of the pattern was given in detail in our previous work.[26] Therefore, only a brief interpretation is given here. The scattering pattern of three-dimensional crystalline structures can be conveniently discussed in terms of the Ewald construction. For an axisymmetric structure the spheres obtained in reciprocal space for isotropic polycrystalline structures become rings obtained by rotating the reciprocal lattice around the symmetry axis. Because the radius of the Ewald sphere ($1/\lambda$) is much larger than the diameter of these reciprocal rings, the Ewald sphere is nearly flat in the region considered, i.e. the Ewald sphere can be considered as a plane. Hence when the sample is irradiated by the X-ray beam perpendicular to the symmetry axis, all reciprocal lattice vectors are intersected by the plane. This yields the SAXS patterns in Figure 2a.

Stretching an fcc structure along its c-axis results in a face-centered tetragonal (fct) structure. However, fct is not a Bravais lattices. It can be divided into body-centered tetragonal (bct) unit cells that contain fewer lattice sites.[28] The indices of the crystallographic planes in an fct structure change when considering the corresponding bct lattice. For the sake of clarity the Miller indices of an fcc lattice were used to analyze the data in the present case. According to the relationship between the representations of crystals in real and reciprocal spaces for any family of lattice planes separated by a distance d there are reciprocal lattice vectors perpendicular to the planes, the shortest of which with a length of $2\pi/d$. Therefore, stretching a crystal in real space corresponds to compressing the reciprocal lattice in the same direction in reciprocal space. Figure 2b shows the SAXS pattern of the uniaxially stretched fiber symmetric sample (left) and the corresponding theoretical structure factor (right). The quantity of the diffraction spots did not change in the course of stretching.

As was mentioned above, the scattering intensity can be expressed as $I(q) \propto S(q) \times P(q)$. The type of Bravais lattice and the form of the single particles change while stretching, leading to a simultaneous changes in $S(q)$ and $P(q)$. On the basis of the present experimental results it is safe to assume that the $S(q)$ and $P(q)$ vary similarly with respect to local deformation on the microscopic level resulting in an invariant quantity of the diffraction spots.

The reciprocal lattice is always centrosymmetric regardless whether the crystal has a symmetry center or not. As can be seen, all the scattering patterns are centrosymmetric in the present case (Figure 1). As mentioned above, they are also axisymmetric after stretching along the fiber axis. However, a different behavior was observed when the sample was stretched along a direction inclined by angles of 35 or 55° with respect to the fiber axis. The diffraction patterns lost their initial axisymmetry. A detailed illustration of this effect (Figure S1) can be found in the Supporting Information. Theoretically, it can be explained using the following equation:[21,29]

$$\tan \vartheta' = \lambda_c^{3/2} \tan \vartheta \qquad (1)$$

where ϑ and ϑ' are the azimuthal angles between scattering vector and the stretching direction before and after deformation, respectively, and λ_c is the microscopic crystalline deformation ratio. When the stretching direction is inclined with respect to the fiber axis, the symmetry of the diffraction spots with respect to the fiber axis is lost. This leads to unequal ϑ values for these diffraction spots and thus unequal shift of the Bragg spots upon stretching due to the nonlinear feature of eq 1.

Affine vs Nonaffine Deformation. The microscopic deformation of the crystallites can be directly obtained by considering the variation of q values of the diffraction spots during stretching. A simple approach is to take the diffraction spots that are located on either the equatorial or the meridian direction with respect to the stretching direction. In the present three cases, as can be seen from figure 1, there are always diffraction spots located perpendicularly to the stretching direction. When the stretching direction is inclined with respect to the fiber axis by angles of 0 and 55°, one pair of the (111) diffraction spots is located perpendicularly to the stretching direction whereas one pair of the (220) diffraction spots is located at this direction when the stretching direction

is inclined by an angle of 35°. Therefore, the positions of these diffraction spots were followed during deformation to evaluate the actual microscopic compression ratio ($\lambda_{c,v} = q_{hkl,0}/q_{hkl,\lambda}$, where $q_{hkl,0}$ and $q_{hkl,\lambda}$ are q values for those hkl planes located perpendicular to the stretching direction. The subscript 0 and λ denote undeformed state and a state of the sample being macroscopically stretched to a draw ratio of λ.). Because of the negligible changes in volume of the latex fibers during deformation, the corresponding draw ratio of the crystallites can be obtained as $1/\lambda_{c,v}^2$. The thus obtained microscopic deformation ratio is compared to the macroscopic one ($\lambda_{m,h}$) as presented in Figure 3a. Included also in Figure 3a are the data derived from an experiment where an isotropic polycrystalline sample made from the same dispersion was stretched.[24]

As was reported previously, deviations from affine microscopic deformation of the crystalline structure with respect to the macroscopic one are observed for isotropic samples. Only at very small macroscopic deformations could the microscopic structure follow affinely. This deformational behavior was explained as follows: the macroscopic deformation is accomplished by the deformation of the colloidal crystalline structure at small draw ratios and slippage between rows of particles and along crystalline grain boundaries at large draw ratios.[23] This means that adhesive forces between latex particles in the film are strong enough to keep the integrity of the entire film with respect to the externally applied stress at small draw ratios whereas they are not strong enough to prevent slippage at large draw ratios. When considering the fiber-symmetric samples investigated here a peculiar effect is observed, cf. Figure 3a. The degree to which the systems adhere to affinity depends on the stretching direction. When the sample was stretched along a direction inclined at angles of 0 or 55° with respect to the fiber axis, the microscopic deformation is closer to affine deformation than when the stretching direction is inclined at 35°. Interestingly, the data of the isotropic polycrystalline sample are located just in between these two cases. This result indicates that the crystallites react in response to the external stress field differently when being stretched along different directions. The behavior of the isotropic polycrystalline sample might thus be considered as an average of the contributions of crystallites with different orientations.

Before considering the structural reasons for the different degrees of affinity of the oriented sample stretched along different directions, we check the effect of annealing on the deformation behavior. Figure 3b shows the microscopic deformation ratio as a function of the macroscopic deformation for samples that were annealed at 100 °C for 4 h. Previous results on the isotropic polycrystalline sample indicate that under this annealing condition the cohesive bonding forces between latex particles in the film promoted by an interdiffusion of polymeric chains across the boundaries of adjacent particles are strong enough to prevent any possible slip process between rows of particles or crystalline grain boundaries. It is thus not surprising that the deformational behavior is in all cases completely affine irrespective of the stretching directions.

To find a structural interpretation for the different degrees of affinity of the oriented soft colloidal crystalline latex film stretched along different directions, we must consider the geometry of crystalline packing in the system. Intuitively it is clear that the crystallographic (111) plane, the plane of densest packing in an fcc structure, must play a special role. On the one hand, as was already shown in Figure 1, when the stretching direction was at 0 or 55° with respect to the fiber axis, the force was applied along in plane with the

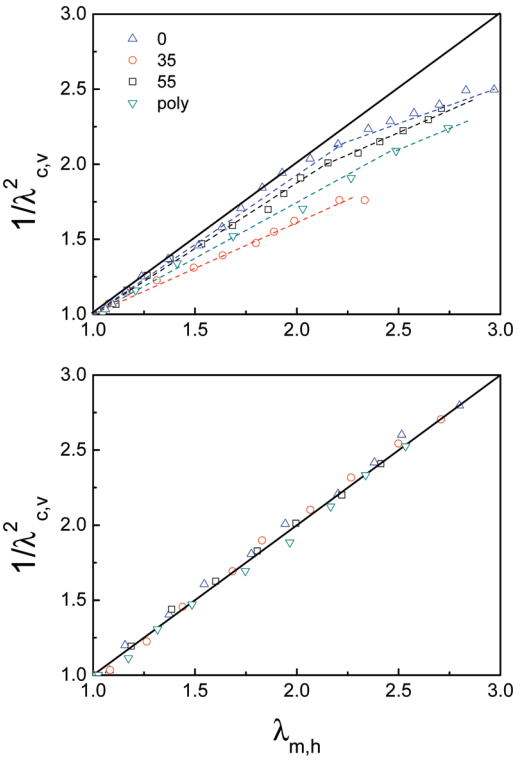

Figure 3. Crystallographic deformation ratios of the colloid crystallites measured perpendicular ($1/\lambda_{c,v}^2$) to the stretching direction as a function of the macroscopic draw ration ($\lambda_{m,h}$) (top). Data for samples after being annealed at 100 °C for 4 h showing a complete affine behavior of the microscopic deformation with respect to the macroscopic one (bottom). The solid line in both plots indicates the behavior expected for affine deformation. Dotted lines are guides for the eyes.

crystallographic (111) plane meaning that all particles in the system were located in parallel planes of densest packing along the stretching direction. In this a case slip processes of interparticle or grain boundaries are largely suppressed. On the other hand, when the stretching direction was at an angle of 35° with respect to the fiber axis, all crystallographic (111) planes are inclined with respect to the stretching direction which eases the slip processes. This is evident if we consider the relative orientations of the direction of maximum shear stress being 45° inclined with respect to the tensile direction and the crystallographic (111) planes. In the case of the isotropic polycrystalline sample the calculation of the degree of affinity was based on the diffraction data of those crystallites which were oriented such that the normal of their crystallographic (111) planes were perpendicular to the stretching direction. However, these crystallites are embedded in a matrix of crystallites of random orientation with different mechanical response. As a consequence, the microscopic deformation of these specific crystallites is less affine than in an oriented sample.

Deformation of the Crystalline Structure. In the discussion of the deformation mechanism above, a simplified approach was chosen: only the diffraction spots located perpendicular to the stretching direction were considered for the calculation of the microscopic deformation ratio. In order to extract further information from the diffraction patterns also positional changes of the diffraction spots located at arbitrary angles with respect to the stretching direction during deformation were considered. This way the behavior of individual crystallites after deformation could be investigated and it could be determined, e.g., whether the crystallites deform homogenously without distortion under stretching.

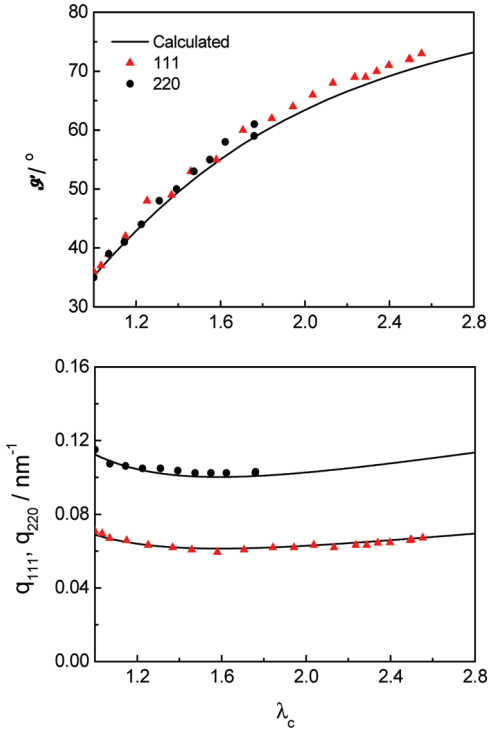

Figure 4. Variation of the azimuthal angles between scattering vector and stretching direction as a function of microscopic draw ratio (λ_c) (top); Plots of q vs λ_c of crystallites stretched along the diagonal of a face and along the body diagonal of fcc crystallites (bottom). Solid lines are calculated values according to eq 1 (top) and eqs 2 and 3 (bottom).

In principle, as was pointed out above, changes in the azimuthal positions after deformation can be easily obtained according to eq 1 provided that the microscopic deformation ratio of the corresponding crystallites is known. However, if the samples were stretched along an arbitrary direction and if the microscopic deformation was nonaffine with respect to the macroscopic one, it would be difficult to obtain the actual microscopic deformation ratio from the diffraction patterns. The problem was simplified in our case due to the fiber symmetric orientation of the crystallites in the sample. Obviously, the variation of crystallographic parameters for an arbitrary group of (hkl) planes as a function of the microscopic deformation ratio in the first two cases of our experiments is straightforward. For the first case, when stretching along the fiber axis, i.e. the normal of the crystallographic (220) plane, the sample was deformed along a face diagonal of the fcc crystallites. This leads to[25]

$$q_{hkl,\lambda_c} = \frac{2\pi}{a}\sqrt{\frac{2h^2 + \lambda_c{}^3 l^2}{\lambda_c{}^2}} \qquad (2)$$

where a is the lattice parameter of the undeformed fcc structure. For the second case, when being stretched at angle of 35° inclined with respect to the fiber axis, i.e., along the body diagonal of the fcc crystallites, one obtains[25]

$$q_{hkl,\lambda_c} = \frac{2\pi}{a}\sqrt{\frac{(h^2 + k^2 + l^2)(2\lambda_c{}^3 + 1) + 2(hk + kl + hl)(1 - \lambda_c{}^3)}{3\lambda_c{}^2}} \qquad (3)$$

To check the validity of the above equations, plots of the azimuthal angle and the q values of selected diffraction spots as a function of microscopic deformation ratio (λ_c) are given in Figure 4. The agreement between the experimental data and the theoretical values is good.

Conclusions

The deformation mechanism of a styrene/*n*-butyl acrylate copolymer latex fiber with fiber symmetric crystalline structure subjected to uniaxial stretching along different directions with respect to its fiber axis was studied by *in situ* synchrotron SAXS. Because of the softness of the constituting latex particles, the scattering spots previously located on circular rings in the undeformed state they lie on ellipses after deformation. The symmetry of the SAXS patterns was changed from fiber symmetry to centrosymmetry only when the stretching direction is not along the fiber axis as it should be according to a simple geometrical consideration of the changes of the reciprocal lattice after deformation. For nonannealed samples the extent of affinity of the microscopic deformation of the crystalline lattices with respect to macroscopic deformation of the bulk samples depended on the stretching directions. This peculiar effect was attributed to the relative orientation of the close packed crystallographic (111) planes. Our results enable a direct comparison between the theoretical considerations and experimental data on the variation of the scattering vectors both in azimuthal distributions and their absolute values as a function of microscopic deformation ratio. It turns out that the experimental data fully agree with theoretical considerations.

Acknowledgment. Y.M. thanks the "Hundred-Talent Project" of the Chinese Academy of Sciences, National Science Foundation of China (20874101, 50621302) and HASYLAB projects (II-20052011, II-20080190). We thank Dr. A. Timmann for assistance in SAXS experiments at HASYLAB.

Supporting Information Available: Figure showing the loss of initial axissymmetry of the diffraction patterns when the samples were stretched along a direction inclined with respect to the fiber axis. This material is available free of charge via the Internet at http://pubs.acs.org.

References and Notes

(1) Keddie, J. L. *Mater. Sci. Eng. R.* **1997**, *21*, 101.
(2) Steward, P. A.; Hearn, J.; Wilkinson, M. C. *Adv. Colloid Interface Sci.* **2000**, *86*, 195.
(3) Winnik, M. A. *Curr. Opin. Colloid Interface Sci.* **1997**, *2*, 192.
(4) Rieger, J.; Hadicke, E.; Ley, G.; Lindner, P. *Phys. Rev. Lett.* **1992**, *68*, 2782.
(5) Chevalier, Y.; Pichot, C.; Graillat, C.; Joanicot, M.; Wong, K.; Maquet, J.; Lindner, P.; Cabane, B. *Colloid Polym. Sci.* **1992**, *270*, 806.
(6) Roulstone, B. J.; Wilkinson, M. C.; Hearn, J.; Wilson, A. J. *Polym. Int.* **1991**, *24*, 87.
(7) Roulstone, B. J.; Wilkinson, M. C.; Hearn, J. *Polym. Int.* **1992**, *27*, 43.
(8) Wang, Y.; Juhue, D.; Winnik, M. A.; Leung, O. M.; Goh, M. C. *Langmuir* **1992**, *8*, 760.
(9) Ming, Y. Q.; Takamura, K.; Davis, H. T.; Scriven, L. E. *Tappi J.* **1995**, *78*, 151.
(10) Ma, Y.; Davis, H. T.; Scriven, L. E. *Prog. Org. Coat.* **2005**, *52*, 46.
(11) Keddie, J. L.; Meredith, P.; Jones, R. A. L.; Donald, A. M. *Macromolecules* **1995**, *28*, 2673.
(12) Winnik, M. A.; Feng, J. R. *J. Coat. Technol.* **1996**, *68*, 39.
(13) Ugur, S.; Holl, Y. *e-Polym.* **2006**, 037.
(14) Park, Y. J.; Lee, D. Y.; Khew, M. C.; Ho, C. C.; Kim, J. H. *Colloids Surf., A* **1998**, *139*, 49.
(15) Lin, F.; Meier, D. J. *Langmuir* **1996**, *12*, 2774.
(16) Rharbi, Y.; Cabane, B.; Vacher, A.; Joanicot, M.; Boue, F. *Europhys. Lett.* **1999**, *46*, 472.

(17) Oberdisse, J. *Macromolecules* **2002**, *35*, 9441.
(18) Lepizzera, S.; Pith, T.; Fond, C.; Lambla, M. *Macromolecules* **1997**, *30*, 7945.
(19) Lepizzera, S.; Scheer, M.; Fond, C.; Pith, T.; Lambla, M.; Lang, J. *Macromolecules* **1997**, *30*, 953.
(20) Fava, D.; Fan, Y. S.; Kumacheva, E.; Winnik, M. A.; Shinozaki, D. M. *Macromolecules* **2006**, *39*, 1665.
(21) Rharbi, Y.; Boue, F.; Joanicot, M.; Cabane, B. *Macromolecules* **1996**, *29*, 4346.
(22) Oberdisse, J.; Rharbi, Y.; Boue, F. *Comput. Theor. Polym. Sci.* **2000**, *10*, 207.
(23) Men, Y. F.; Rieger, J.; Roth, S. V.; Gehrke, R.; Kong, X. M. *Langmuir* **2006**, *22*, 8285.
(24) Zhang, J. Q.; Hu, S. S.; Rieger, J.; Roth, S. V.; Gehrke, R.; Men, Y. F. *Macromolecules* **2008**, *41*, 4353.
(25) Zhang, J. Q.; Men, Y. F. *Chin. J. Polym. Sci.* **2009**, *27*, 49.
(26) Hu, S. S.; Men, Y. F.; Roth, S. V.; Gehrke, R.; Rieger, J. *Langmuir* **2008**, *24*, 1617.
(27) Hu, S. S.; Rieger, J.; Lai, Y. Q.; Roth, S. V.; Gehrke, R.; Men, Y. F. *Macromolecules* **2008**, *41*, 5073.
(28) Cawley, J. D. *NASA Technical Paper* 1984, art. no. 2286.
(29) Kratky, O. *Kolloid Z.* **1933**, *64*, 213.